Hot Paper + Inside Cover: Metallic Single-Unit-Cell Orthorhombic Cobalt Diselenide Atomic Layers: Robust Water-Electrolysis Catalysts

ARTICLE *in* ANGEWANDTE CHEMIE · OCTOBER 2015

DOI: 10.1002/ange.201505245

Water Splitting Hot Paper

Deutsche Ausgabe: DOI: 10.1002/ange.201505245
Internationale Ausgabe: DOI: 10.1002/anie.201505245

Metallic Single-Unit-Cell Orthorhombic Cobalt Diselenide Atomic Layers: Robust Water-Electrolysis Catalysts

Liang Liang, Hao Cheng, Fengcai Lei, Jun Han, Shan Gao, Chengming Wang, Yongfu Sun, Shaista Qamar, Shiqiang Wei,* and Yi Xie**

Abstract: *The bottleneck in water electrolysis lies in the kinetically sluggish oxygen evolution reaction (OER). Herein, conceptually new metallic non-metal atomic layers are proposed to overcome this drawback. Metallic single-unit-cell $CoSe_2$ sheets with an orthorhombic phase are synthesized by thermally exfoliating a lamellar $CoSe_2$-DETA hybrid. The metallic character of orthorhombic $CoSe_2$ atomic layers, verified by DFT calculations and temperature-dependent resistivities, allows fast oxygen evolution kinetics with a lowered overpotential of 0.27 V. The single-unit-cell thickness means 66.7% of the Co^{2+} ions are exposed on the surface and serve as the catalytically active sites. The lowered Co^{2+} coordination number down to 1.3 and 2.6, gives a lower Tafel slope of 64 mV dec^{-1} and higher turnover frequency of 745 h^{-1}. Thus, the single-unit-cell $CoSe_2$ sheets have around 2 and 4.5 times higher catalytic activity compared with the lamellar $CoSe_2$-DETA hybrid and bulk $CoSe_2$.*

Nowadays, over 90% of hydrogen is obtained by reforming fossil fuels, a process which consumes fossil resources and simultaneously produces carbon dioxide, thus exacerbating the energy crisis and increasing the risk of global warming.[1] An attractive alternative for H_2 production is the electrocatalytic water splitting which involves no fossil fuels and produces no greenhouse gases. Water electrolysis consists of two half reactions: 1) water oxidation [$H_2O \rightarrow 1/2\,O_2 + 2\,H^+ + 2\,e^-$] and 2) proton reduction [$2\,H^+ + 2\,e^- \rightarrow H_2$]. The first half reaction is generally considered as the critical bottleneck in developing efficient electrolysis of water owing to the inherent sluggish oxygen evolution reaction (OER) kinetics.[2] This OER process involves a four-electron transfer associated with O–H bond breaking and O–O bond formation, which usually imposes a high overpotential requirement and hence seriously hinders large-scale hydrogen production from water splitting. Researchers have demonstrated that, benefiting from the high electronic conductivity, a few noble metals, such as Ru, Ir, could overcome this drawback of very low OER kinetics and hence exhibit superior OER activity,[3] however, the rapid deactivation, high cost, and low abundance unfortunately impede their commercial utilization. Although many earth-abundant transition-metal (Fe, Co, Ni, Mn) oxides[2b–d,4a] and chalcogenides[4b,c] have exhibited long-term structural stability during the OER measurements, all of them usually suffer from low catalytic activities as well as high overpotentials, which is primarily attributed to their inherently poor electrical conductivity and very low number of exposed surface active sites. Therefore, developing an ideal catalyst material with high conductivity, abundant active sites, and robust stability holds the key to achieving a breakthrough in water electrolysis technology.

To achieve this important goal, we first construct an ideal material model of metallic non-metal atomic layers. Owing to the atomic thickness, the unique structure can expose an ultrahigh fraction of low-coordinated surface atoms that are comparable with the total atoms, which could serve as the active sites to efficiently catalyze the oxygen evolution reactions.[5] In addition, the structure distortion that usually occurs in atomically thin 2D structures has been demonstrated to decrease the surface energy and hence favor favorable structural stability.[6] Importantly, in spite of circumventing the utilization of noble metals, these structures still have metallic character, which allows quick reaction kinetics for water oxidation along the 2D atomic layers and hence improves the OER activity. In this regard, our theoretical investigations reveal that the transition-metal chalcogenide of orthorhombic $CoSe_2$ with single-unit-cell thickness would be a promising contender. For the orthorhombic $CoSe_2$, Co atoms are octahedrally bonded to adjacent Se atoms, while the adjacent octahedra are edge-shared to form a 3D macarsite-type crystal structure.[7] Density functional theory (DFT) calculations divulge the metallic behavior of the single-unit-cell orthorhombic $CoSe_2$ atomic layers, in which the density of states (DOS) resides across the Fermi level (Figure 1 A,C), giving promising signs for high microscopic 2D conductivity. To verify the theoretically metallic conductance, temperature-dependent resistivity measurements of the thin film are carried out. As shown in Figure 1 B, with increasing temperature the electric resistivity gradually increased, showing the typical metallic conducting

[*] L. Liang,[+] F. Lei, S. Gao, Dr. C. Wang, Prof. Y. Sun, S. Qamar, Prof. Y. Xie
Hefei National Laboratory for Physical Sciences at Microscale
Collaborative Innovation Center of Chemistry for Energy Materials
University of Science & Technology of China
Hefei, Anhui 230026 (P.R. China)
E-mail: yfsun@ustc.edu.cn
yxie@ustc.edu.cn
Dr. H. Cheng,[+] Prof. S. Wei
National Synchrotron Radiation Laboratory
University of Science and Technology of China
Hefei, Anhui 230029 (P.R. China)
E-mail: sqwei@ustc.edu.cn
Dr. J. Han
Paul Scherrer Institut
5232 Villigen PSI (Switzerland)
[+] These authors contributed equally to this work.

Supporting information for this article is available on the WWW under http://dx.doi.org/10.1002/anie.201505245.

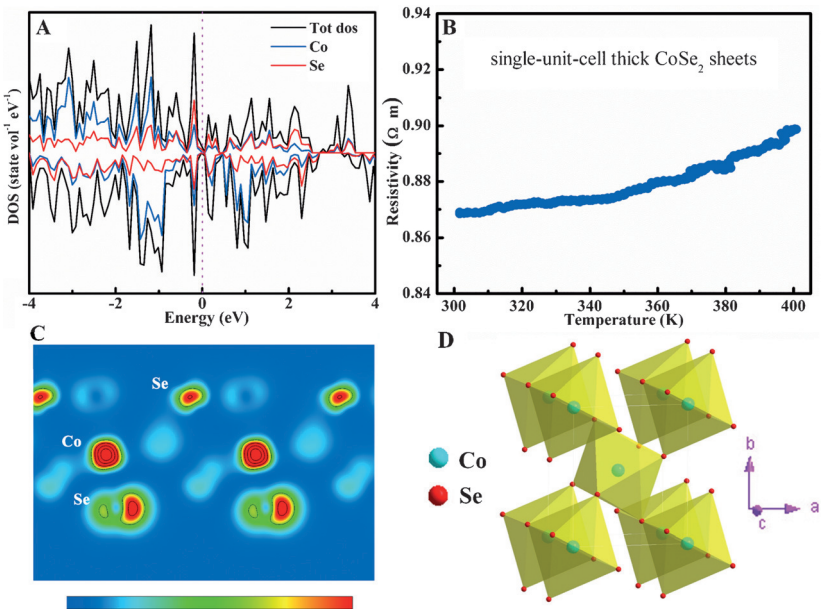

Figure 1. A) Calculated density of states (DOS) and C) the corresponding charge-density contour at the Fermi level for single-unit-cell orthorhombic $CoSe_2$ atomic layers; B) temperature-dependent resistivity of single-unit-cell orthorhombic $CoSe_2$ atomic layers based thin film; D) unit cell structure of orthorhombic $CoSe_2$.

behavior and confirming the metallicity of single-unit-cell orthorhombic $CoSe_2$ atomic layers. Moreover, according to previous studies by Shao-Horn et al,[8] orthorhombic $CoSe_2$ with a $t_{2g}^6e_g^1$ electronic configuration near an optimal e_g filling would be an ideal candidate for highly efficient OER electrocatalysts. Thus, it is highly desirable to fabricate single-unit-cell $CoSe_2$ layers with an orthorhombic phase. In spite of the recent synthesis of $CoSe_2$ nanosheets with a cubic phase,[4c] the strong in-plane bonds and the poor intrinsic driving force for 2D anisotropic growth make the synthesis of non-layered orthorhombic $CoSe_2$ (Figure 1D) atomic layers to be a huge challenge. Hence, significant further efforts are still needed to establish a facile and convenient strategy for fabricating orthorhombic $CoSe_2$ atomic layers with a single-unit-cell thickness.

Herein, clean and freestanding single-unit-cell thick $CoSe_2$ sheets with non-layered orthorhombic structure have been successfully synthesized through heating the artificially fabricated lamellar hybrid $CoSe_2$-DETA (DETA = diethylenetriamine) intermediate (Figure 2A), this is the first example of the synthesis of orthorhombic $CoSe_2$ ultrathin sheets. The DETA benefits the formation of lamellar hybrid 1D structures (Figure S1), while simultaneously the oleate ions tend to adsorb on their lateral side and hence facilitate their crystal growth to 2D plate-like morphology (Figure S2 in the Supporting Information).[5a,9] The small-angle X-ray scattering (SAXS) pattern shown in Figure 2B demonstrates the high degree of ordering within this lamellar hybrid intermediate. In addition, the series of "00L" X-ray diffraction peaks further provide direct evidence for the presence of an ordered mesostructure with a layer spacing of 1.1 nm, which agrees with the interlayer distance of approximately 1.06 nm revealed by the corresponding lateral TEM image (Figure 2B).[6a,10] Meanwhile, X-ray photoelectron spectroscopy (XPS) and FT-IR spectra in Figure S3A, S4 demonstrate the presence of DETA and oleate ions in the intermediate products.[4b,5c] And then, upon heating at 350 °C for 1 h in air, the lamellar hybrid $CoSe_2$-DETA intermediate could be fully exfoliated into freestanding single-unit-cell thick $CoSe_2$ sheets (Figure S5). The XRD pattern of the obtained products in Figure S5B could be readily indexed to orthorhombic $CoSe_2$, corresponding to JCPDS No. 53-0449. In addition, the corresponding XPS and FT-IR spectra in Figure S6, S4 demonstrate the absence of DETA and $C_{18}H_{33}NaO_2$, giving direct evidence for the formation of clean and pure $CoSe_2$. The TEM image in Figure S5A illustrates their uniform freestanding and large-area graphene-like morphology with lateral size of around 300 nm. The HRTEM image in Figure 2C reveals their [010] orientation of the synthesized orthorhombic $CoSe_2$ sheets. Atomic force microscopic (AFM) and the corresponding height profile in Figure 2D, E clearly shows that their average thickness of around 0.66 nm, which agrees well with the thickness of single-unit-cell thick $CoSe_2$ slab along the [010] direction. Therefore, all the above results unambiguously demonstrate the formation of clean and freestanding single-unit-cell thick orthorhombic $CoSe_2$ sheets.

To unravel the local atomic arrangements, bond lengths and coordination numbers of the synthetic single-unit-cell thick $CoSe_2$ sheets,[11] synchrotron radiation X-ray absorption fine structure (XAFS) measurements are performed. The Co K-edges $k^3\chi(k)$ oscillation curves in Figure 3A show clear differences among the single-unit-cell thick $CoSe_2$ sheets, $CoSe_2$-DETA hybrid intermediate, and bulk $CoSe_2$ (Figure S7), implying their distinct local atomic arrangement, further demonstrated by their R-space curves in Figure 3B. The FT curves for all the three products display one main peak, which corresponds to the nearest Co–Se coordination (Figure 3B). For the single-unit-cell thick $CoSe_2$ sheets, the Co–Se peak is shifted to 2.09 Å along with a decrease in peak intensity, compared with the other two products. This result could be further verified by their Se K-edge data, that is, the Se–Co peak position is shifted to the lower-R side and the peak intensity is greatly reduced for the single-unit-cell thick $CoSe_2$ sheets with regard to bulk $CoSe_2$ (Figure 3B). According to the high-quality extended XAFS spectra, least-squares fittings are further conducted and the obtained quantitative results are shown in Figure 3C. For the $CoSe_2$-DETA hybrid intermediate, the bond lengths and coordination numbers of Co–Se decrease remarkably, while their disorder degrees increase significantly as compared with bulk counterpart, suggesting that the Co–N coordination results in a noticeable distortion on the surface. In addition, after exfoliating into the single-unit-cell thick $CoSe_2$ sheets, the surface Co atoms inherit the coordination number of 1.3 and 2.6 for the $CoSe_2$-

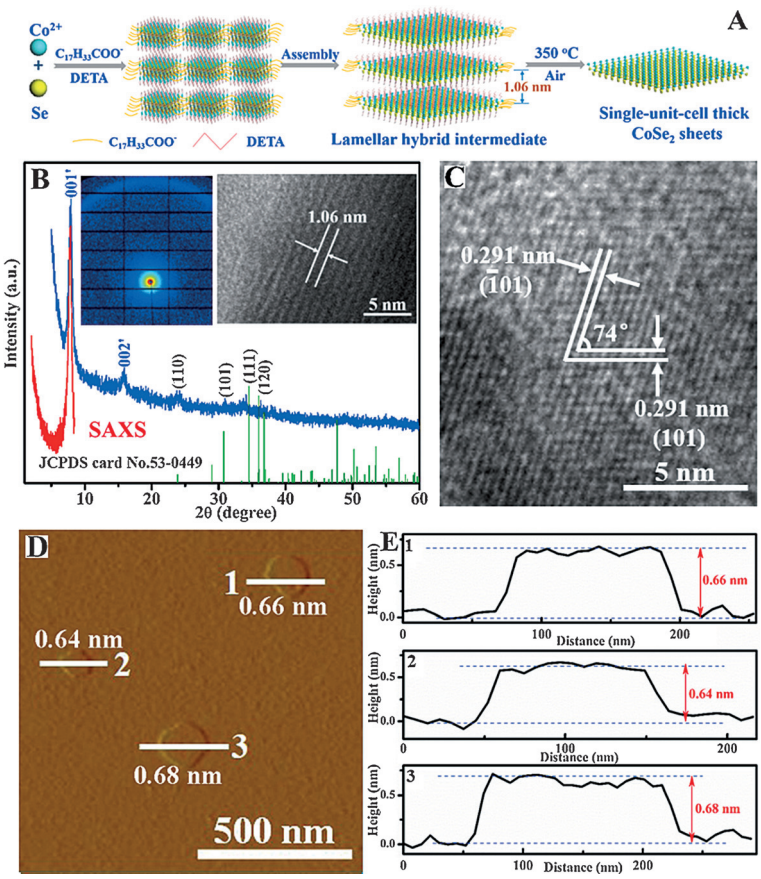

Figure 2. A) Schematic illustration for fabricating [010]-oriented single-unit-cell thick $CoSe_2$ sheets, taking advantage of the lamellar hybrid $CoSe_2$-DETA intermediate; B) the SAXS profile (red line and inset left image), XRD pattern (blue line) and the corresponding lateral TEM image for the lamellar hybrid $CoSe_2$-DETA intermediate; characterizations for the single-unit-cell thick $CoSe_2$ sheets C) HRTEM image, D) AFM image and E) the corresponding height profiles, the numbers 1 to 3 in (E) correspond to the numbers 1 to 3 in (D).

DETA hybrid, while their bond lengths and disorder degrees further increase remarkably, indicating that the exfoliation process aggravates the surface structure distortion. Such clear structure distortion would bring about excellent structural stability through decreasing the surface energy.[5a,b,6]

Thanks to the metallic character, atomic thickness, lowered coordination number, as well as the structural distortion, the metallic single-unit-cell thick $CoSe_2$ sheets should give improved electrochemical oxidation of water to oxygen.[2,12] As expected, the bare glassy carbon (GC) electrode is totally inactive towards O_2 production. Intriguingly, the single-unit-cell thick $CoSe_2$ sheets show an initial O_2 evolution at a very small overpotential (η) of 0.27 V, smaller than that of lamellar hybrid $CoSe_2$-DETA intermediate (0.33 V) and bulk $CoSe_2$ (0.38 V; Figure 4A). At $\eta = 0.47$ V, the current density of single-unit-cell thick $CoSe_2$ sheets is 73 mA cm^{-2}, which is 2 and 4.5 times higher than that of lamellar hybrid $CoSe_2$-DETA intermediate and bulk $CoSe_2$, respectively, strongly demonstrating the high electrocatalytic activity of 2D structure with single-unit-cell thickness. Also, the single-unit-cell thick $CoSe_2$ sheets show a Tafel slope of 64 mV dec^{-1} (Figure S8A), smaller than that of lamellar hybrid $CoSe_2$-DETA intermediate and bulk $CoSe_2$, demonstrating their faster kinetics of water oxidation.[2] Moreover, the single-unit-cell thick $CoSe_2$ sheets exhibit the highest turnover frequency (TOF) of 745 h^{-1} at $\eta = 0.47$ V, which is roughly 2 and 4.5 times higher than that of lamellar hybrid $CoSe_2$-DETA intermediate and bulk $CoSe_2$, respectively, indicating the single-unit-cell thick $CoSe_2$ sheet's better intrinsic catalytic activity. Furthermore, the steady-state current densities of the single-unit-cell thick $CoSe_2$ sheets still remain constant even after 2 days (Figure 4B and Figure S9), providing solid evidence for long-term stability and hence showing perspective signs for practical applications.

Of note, the greatly improved electrocatalytic performances of single-cell-unit thick $CoSe_2$ sheets could be credited to their metallic character, ultralarge fraction of surface atoms with lowered coordination number, and clear structural distortion. As revealed by the DFT calculations and temperature dependent-resistivities in Figure 1A,B, the single-unit-cell thick orthorhombic $CoSe_2$ sheets have the necessary metallic character, which favors the 4e$^-$ transfer kinetics during water oxidation (Figure S8B) and hence reduces the overpotential down to 0.27 V. Moreover, as the thickness is down to single-cell-unit thick, the synthesized $CoSe_2$ atomic layers can expose 66.7% of the Co^{2+} ions on the surface, which could serve as active sites for accelerating the water oxidation reaction.[12] This can be further verified by the correlation between their electrochemically active surface area (ECSA) and catalytic activity.[13] The lamellar $CoSe_2$-DETA hybrid exhibits an 11-times larger ECSA than bulk $CoSe_2$, while having only a 2.25-times higher catalytic current (Figure 4C), which indicates that the organic ligands between the $CoSe_2$ layers prevent the electron transport along the thickness direction. Upon exfoliating into clean single-unit-cell thick $CoSe_2$ sheets, they achieve a 1.6-times higher ECSA compared with the $CoSe_2$-DETA hybrid, which is consistent with their roughly 2-times higher catalytic current, strongly demonstrating that the increased active sites benefit electrocatalytic activity. Furthermore, synchrotron radiation XAFS results in Figure 3C reveal that the Co–N coordination lowers the surface Co coordination number down to 1.3 and 2.6, and hence inevitably leads to a clear structural distortion. With the removal of DETA ligands, the single-unit-cell thick $CoSe_2$ sheets preserve the surface Co coordination number as well as causing a further distorted structure. The lowered Co coordination number endows the single-unit-cell thick $CoSe_2$ sheets with many dangling bonds, which benefit for higher intrinsic catalytic activity,[14] demonstrated by their lower Tafel slope of 64 mV dec^{-1} and higher TOF of 745 h^{-1}. In addition, the better intrinsic catalytic activity for the single-unit-cell thick $CoSe_2$ sheets could be further confirmed by their highest slope of catalytic activity versus ECSA in Figure 4D, suggesting that their electrocatalytic current

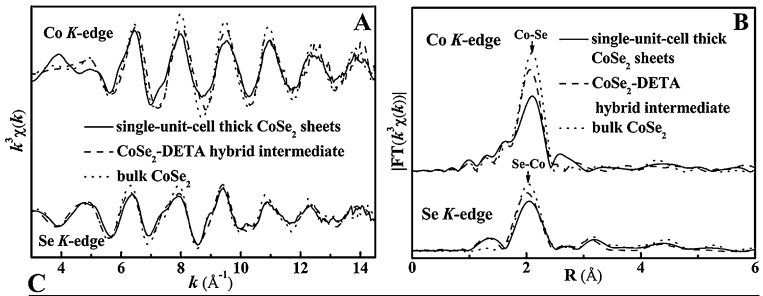

C

Sample	Path	N	R (Å)	σ^2 (10^{-3}Å^2)	ΔE_0 (eV)
bulk $CoSe_2$	Co-Se_1	2.0	2.35	4.5	2.5
	Co-Se_2	4.0	2.40	4.7	2.5
	Se-Co_1	1.0	2.35	5.1	3.3
	Se-Co_2	2.0	2.40	5.4	3.3
$CoSe_2$-DETA hybrid	Co-N	0.2	1.97	3.3	1.6
	Co-Se_1	1.3	2.33	4.9	2.4
	Co-Se_2	2.6	2.38	5.0	2.4
	Se-Co_1	1.0	2.33	5.8	3.4
	Se-Co_2	1.9	2.37	6.2	3.4
single-unit-cell thick $CoSe_2$ sheets	Co-Se_1	1.3	2.38	5.2	2.5
	Co-Se_2	2.6	2.42	5.7	2.5
	Se-Co_1	0.9	2.37	6.7	3.4
	Se-Co_2	1.9	2.42	7.4	3.4

Figure 3. A) Co K-edge and Se K-edge extended XAFS oscillation function $k^3\chi(k)$, B) the corresponding Fourier transforms FT($k^3\chi(k)$), C) structural parameters around Co and Se atoms extracted from EXAFS curve-fitting for the single-unit-cell thick $CoSe_2$ sheets, $CoSe_2$-DETA hybrid intermediate and bulk $CoSe_2$.

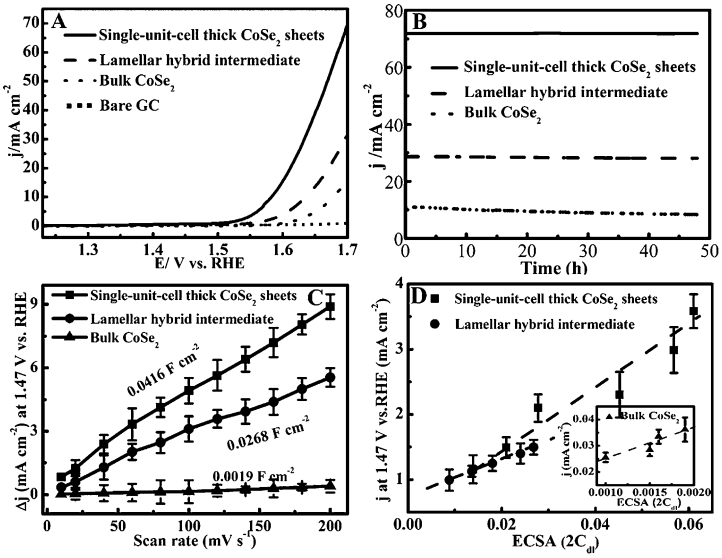

Figure 4. Electrochemical properties for the single-unit-cell thick $CoSe_2$ sheets, lamellar hybrid $CoSe_2$-DETA intermediate, and bulk $CoSe_2$: A) polarization curves; B) *I*–*t* curve at 1.7 V versus reversible hydrogen electrode (RHE); C) the differences in current density variation ($\Delta j = j_a - j_c$) at a potential of 1.47 V plotted against scan rate fitted to a linear regression enables the estimation of C_{dl}; D) current density at 1.47 V versus RHE plotted against ECSA for various materials at different loadings.

would increase much faster than that of the other two samples with the increase of ECSA. Besides, the greater structure distortion for single-unit-cell thick $CoSe_2$ sheets helps to improve their structural stability and hence their electrocatalytic activity proceeds without deactivation even after 48 h.[5a,b,6,11]

In summary, conceptually new metallic/nonmetal atomic layers are put forward to overcome the kinetically sluggish oxygen evolution reaction. As an example, metallic single-unit-cell thick $CoSe_2$ freestanding sheets with an orthorhombic phase are synthesized by thermally exfoliating the synthesized lamellar $CoSe_2$-DETA hybrid. The metallic character for the single-unit-cell thick $CoSe_2$ sheets, demonstrated by DFT calculations and temperature-dependent resistivities, allows high electronic conductivity and ensures fast oxygen evolution kinetics with lowered overpotential of 0.27 V. Benefiting from the single-unit-cell thickness, 66.7% Co^{2+} ions could be exposed on the surface and serve as the catalytically active sites, while their lowered coordination numbers of 1.3 and 2.6, revealed by EXAFS fitting results, favors a lower Tafel slope of 64 mV dec^{-1}, higher turnover frequency of 745 h^{-1}, and larger slope of current versus ECSA. As a result, the single-unit-cell thick $CoSe_2$ sheets yield an electrocatalytic current of 73 mA cm^{-2}, roughly 2 and 4.5 times higher than that of lamellar hybrid $CoSe_2$-DETA intermediate and bulk $CoSe_2$, respectively, while the clearly distorted structure enables the sheet's activity to proceed without deactivation even after 48 h. Briefly, this work provides new opportunities for designing efficient and robust water oxidation catalysts.

Acknowledgements

This work was financially supported by National Basic Research Program of China (2015CB932302), National Nature Science Foundation (21331005, 21422107, 21201157, 91422303, 11321503), Program for New Century Excellent Talents in University (NCET-13-0546), Youth Innovation Promotion Association of CAS (CX2340000100), and the Fundamental Research Funds for the Central Universities No. WK2340000063.

Keywords: atomic layers · cobalt diselenide · electrocatalysis · water splitting

How to cite: *Angew. Chem. Int. Ed.* **2015**, *54*, 12004–12008
Angew. Chem. **2015**, *127*, 12172–12176

[1] B. Rausch, M. D. Symes, G. Chisholm, L. Cronin, *Science* **2014**, *345*, 1326.

[2] a) A. Kudo, Y. Miseki, *Chem. Soc. Rev.* **2009**, *38*, 253; b) M. M. Najafpour, T. Ehrenberg, M. Wiechen, P. Kurz, *Angew. Chem. Int. Ed.* **2010**, *49*, 2233; *Angew. Chem.* **2010**, *122*, 2281; c) F. Jiao, H. Frei, *Angew. Chem. Int. Ed.* **2009**, *48*, 1841; *Angew. Chem.* **2009**, *121*, 1873; d) Y. Y. Liang, Y. G. Li, H. L. Wang, J. G. Zhou, J. Wang, T. Regier, H. J. Dai, *Nat. Mater.* **2011**, *10*, 780; e) Y. F. Sun, S. Gao, F. C. Lei, J. W. Liu, L. Liang, Y. Xie, *Chem. Sci.* **2014**, *5*, 3976.

[3] a) M. G. Walter, E. L. Warren, J. R. Mckone, S. W. Boettcher, Q. Mi, E. A. Santori, N. S. Lewis, *Chem. Rev.* **2010**, *110*, 6446; b) J. Wang, H. X. Zhong, Y. L. Qin, X. B. Zhang, *Angew. Chem. Int. Ed.* **2013**, *52*, 5248; *Angew. Chem.* **2013**, *125*, 5356.

[4] a) G. P. Gardner, Y. B. Go, D. M. Robinson, P. F. Smith, J. Hadermann, A. Abakumov, M. Greenblatt, G. C. Dismukes, *Angew. Chem. Int. Ed.* **2012**, *51*, 1616; *Angew. Chem.* **2012**, *124*, 1648; b) M. R. Gao, W. T. Yao, H. B. Yao, S. H. Yu, *J. Am. Chem. Soc.* **2009**, *131*, 7486; c) Y. W. Liu, H. Cheng, M. J. Lyu, S. J. Fan, Q. H. Liu, W. S. Zhang, Y. D. Zhi, C. M. Wang, C. Xiao, S. Q. Wei, B. J. Ye, Y. Xie, *J. Am. Chem. Soc.* **2014**, *136*, 15670.

[5] a) Y. F. Sun, Q. H. Liu, S. Gao, H. Cheng, F. C. Lei, Z. H. Sun, Y. Jiang, H. B. Su, S. Q. Wei, Y. Xie, *Nat. Commun.* **2013**, *4*, 2899; b) Y. F. Sun, Z. H. Sun, S. Gao, H. Cheng, Q. H. Liu, F. C. Lei, S. Q. Wei, Y. Xie, *Adv. Energy Mater.* **2014**, *4*, 1300611; c) F. C. Lei, Y. F. Sun, K. T. Liu, S. Gao, L. Liang, B. C. Pan, Y. Xie, *J. Am. Chem. Soc.* **2014**, *136*, 6826 – 6829.

[6] a) Y. F. Sun, Z. H. Sun, S. Gao, H. Cheng, Q. H. Liu, J. Y. Piao, T. Yao, C. Z. Wu, S. L. Hu, S. Q. Wei, Y. Xie, *Nat. Commun.* **2012**, *3*, 1057; b) Y. F. Sun, H. Cheng, S. Gao, Z. H. Sun, Q. H. Liu, Q. Liu, F. C. Lei, T. Yao, J. F. He, S. Q. Wei, Y. Xie, *Angew. Chem. Int. Ed.* **2012**, *51*, 8727 – 8731; *Angew. Chem.* **2012**, *124*, 8857 – 8861.

[7] D. H. Kong, H. T. Wang, Z. Y. Lu, Y. Cui, *J. Am. Chem. Soc.* **2014**, *136*, 4897.

[8] a) J. Suntivich, K. J. May, H. A. Gasteiger, J. B. Goodenough, Y. Shao-Horn, *Science* **2011**, *334*, 1383; b) J. Kim, X. Yin, K. C. Tsao, S. H. Fang, H. Yang, *J. Am. Chem. Soc.* **2014**, *136*, 14646.

[9] Y. F. Sun, S. S. Jiang, W. T. Bi, R. Long, X. G. Tan, C. Z. Wu, S. Q. Wei, Y. Xie, *Nanoscale* **2011**, *3*, 4394.

[10] S. Gao, Y. F. Sun, F. C. Lei, J. W. Liu, L. Liang, T. W. Li, B. C. Pan, J. F. Zhou, Y. Xie, *Nano Energy* **2014**, *8*, 205 – 213.

[11] Y. F. Sun, S. Gao, Y. Xie, *Chem. Soc. Rev.* **2014**, *43*, 530 – 546.

[12] Y. F. Sun, S. Gao, F. C. Lei, Y. Xie, *Chem. Soc. Rev.* **2015**, *44*, 623.

[13] F. Song, X. L. Hu, *Nat. Commun.* **2014**, *5*, 4477.

[14] a) Y. F. Sun, S. Gao, F. C. Lei, C. Xiao, Y. Xie, *Acc. Chem. Res.* **2015**, *48*, 3; b) Y. F. Sun, H. Cheng, S. Gao, Q. H. Liu, Z. H. Sun, C. Xiao, C. Z. Wu, S. P. Wei, Y. Xie, *J. Am. Chem. Soc.* **2012**, *134*, 20294 – 20297.

Received: June 8, 2015
Published online: July 29, 2015

